Multiple-time-scaling lattice Boltzmann method for the convection diffusion equation

Like Li*
Department of Mechanical Engineering, Mississippi State University, Mississippi State, Mississippi 39762, USA

(Received 18 March 2019; published 3 June 2019)

A multiple-time-scaling (MTS) strategy that decouples the time discretization in different domains and enables flexible time-step coarsening, refinement, and stretching in the lattice Boltzmann method (LBM) for the convection diffusion equation is developed. The key in the multiple-time scaling is the satisfaction of physical interface conditions without nested iterations in each time step by implementing appropriate interface schemes for the distribution functions in the LBM. The applicability and second-order accuracy of the MTS-LBM approach is demonstrated with two numerical tests. Our approach greatly expands the avenue and expedites the progress of applying the LBM for modeling complex flows and transport phenomena involving multiphases and multicomponents with large property ratios.

DOI: 10.1103/PhysRevE.99.063301

I. INTRODUCTION

Fluid flows and thermal and chemical transport involving multiphases and multicomponents are ubiquitous in nature and have wide-ranging applications. Accurate and reliable models for studying these phenomena, however, are still limited due to a number of challenges for both the development and application of computational methods [1–6]. The distinct properties of the different phases or materials, such as large density, viscosity, and thermal and mass diffusivity ratios, require the simulation parameters to vary over a wide range [5,7–11]. In addition, different length scales and timescales are usually necessary to capture the field and interfacial flows and transport, especially for dynamically moving interfaces [3,12]. Advancement in these areas has the potential to substantially improve the applicability and/or accuracy of the numerical models.

The lattice Boltzmann method (LBM) has emerged as an alternative numerical method to model complex flows and transport in homogeneous and single-component media [13–17]. One of the basic features of the LBM is its Cartesian grid system and uniform discretization in both space and time. This makes the LBM an easy-to-start numerical approach with simple formulation and convenient implementation. In the last two decades, the LBM has also witnessed growing success in modeling multiphase and multicomponent flows and transport [4,5,11,18,19], although significant improvement is still warranted for the LBM to model complex interfacial transport phenomena in systems with large ratios of the physical and/or transport properties of the adjacent domains [5,8–10].

First, in order to capture both boundary-layer behaviors and far-field effects on momentum and on thermal and mass transport, nonuniform meshes and/or local grid refinement are usually preferred, to which a considerable amount of effort has been devoted in the LBM literature [12,20;21 and references therein]. Moreover, adaptive or local time stepping is generally necessary to (1) accommodate the spatial grid refinement to ensure numerical stability, and (2) capture both rapid changes (with time-step refinement) and long-time evolving processes (with time-step coarsening). Such nonuniform time-scaling treatment has been widely employed in popular finite-difference or finite-volume methods [22–24]. However, the manipulation of separate or different time steps in modeling transient flows and transport between domains with different properties has not be conducted in the LBM.

In this paper, we propose and demonstrate a multiple-time-scaling (MTS) strategy in the LBM, to realize independent and tunable time scaling in different domains. The MTS strategy incorporates all the aforementioned benefits of adaptive time stepping into the LBM computation; moreover, it decouples the space and time discretization in the LBM, paving the way for applying the LBM to model a variety of complex flow and transport problems. One particular application is for effective modeling of flow and transport between materials and phases of large property ratios; with MTS, the original requirement for corresponding large ratios of the relaxation coefficients in different domains in the LBM is released [see Eqs. (3) and (6)]. Another field of application is for the efficient simulation of transient flows and transport involving both slowly and rapidly evolving processes.

The rest of the paper is organized as follows. In Sec. II, the conventional lattice Boltzmann (LB) model for the general convection diffusion equation (CDE) for transport is briefly reviewed, and the selection of relaxation coefficients in different domains with a single time scaling is discussed. Section III provides the details for developing the MTS strategy. Two numerical tests are presented in Sec. IV to verify the applicability and accuracy of the proposed MTS-LBM approach. And Sec. V concludes the paper.

II. CONVENTIONAL LBM FOR CDE WITH A SINGLE TIME SCALING

To show a direct comparison of the proposed MTS strategy with the conventional single time scaling, we formulate both

*likeli@me.msstate.edu

approaches within the framework of the lattice Boltzmann (LB) model for the general convection diffusion equation (CDE), $\partial_t \phi + \nabla \cdot (\mathbf{u}\phi) = \nabla \cdot (D\nabla\phi) + G$, where ϕ is a scalar variable (e.g., temperature and concentration in thermal and mass transport, respectively), t is the time, $\mathbf{u}$ is the velocity vector, D is the diffusion coefficient, and G is the general source term. In LB models for solving the CDE, a set of microscopic distribution functions, $g(\mathbf{x}, \boldsymbol{\xi}, t)$, is defined in the discrete velocity space, and its evolution is governed by the LB equation (LBE) [16,17],

$$g_\alpha(\mathbf{x} + \mathbf{e}_\alpha\delta_t, t + \delta_t) - g_\alpha(\mathbf{x}, t) = [\mathbf{L} \cdot (\mathbf{g} - \mathbf{g}^{\mathrm{eq}})(\mathbf{x}, t)]_\alpha + \omega_\alpha G(\mathbf{x}, t)\delta_t, \tag{1}$$

where $g_\alpha(\mathbf{x}, t) \equiv g(\mathbf{x}, \boldsymbol{\xi}_\alpha, t)$, $\boldsymbol{\xi}$ is the particle velocity vector and is discretized to a set of discrete velocities $\{\boldsymbol{\xi}_\alpha | \alpha = 0, 1, \ldots, m-1\}$, $\mathbf{e}_\alpha$ is the αth discrete velocity vector, δ_t is the time step, $\mathbf{L}$ is the collision operator such as those in the single-relaxation-time (SRT) and multiple-relaxation-time (MRT) LB models [16,17], $g_\alpha^{\mathrm{eq}}(\mathbf{x}, t)$ is the equilibrium distribution function dependent on the macroscopic velocity and scalar variable, and ω_α is the weight coefficient. The macroscopic scalar variable can be obtained from the moment of the distribution functions as

$$\phi(\mathbf{x}, t) = \sum_{\alpha=0}^{m-1} g_\alpha(\mathbf{x}, t). \tag{2}$$

In the recovered CDE, the thermal or mass diffusivity, D, is related to the respective relaxation coefficient in the LB models as $D = \frac{2\tau-1}{6}\frac{L_x^2}{L_t}$, with $L_x = (\delta_x)_{\mathrm{phys}}/(\delta_x)_{\mathrm{LB}}$ and $L_t = (\delta_t)_{\mathrm{phys}}/(\delta_t)_{\mathrm{LB}}$ the respective length- and time-scaling factors between the physical and LBM unit systems [16,17]. For simplicity, we consider only isotropic diffusion in this paper; extension of the analysis to anisotropic diffusion is straightforward following, e.g., that in [16,17]. The relaxation coefficient τ in the LB model can affect both numerical stability and accuracy, e.g., the lower limit for τ is $\tau > 0.5$ and numerical instability could be encountered when τ is chosen close to 0.5 [25]. On the other hand, larger τ values represent larger time steps, and the magnitude of the numerical errors from LBM solutions would increase when larger τ values are used [26,27].

In previous LB models for simulating flow and transport between different domains, only a single time scaling was used, and the relaxation coefficients in the two domains are related to each other as

$$\frac{2\tau_2 - 1}{2\tau_1 - 1} = \frac{D_2}{D_1}. \tag{3}$$

The relationship in Eq. (3) clearly shows that one has only the choice to choose one relaxation coefficient and the other is determined accordingly. Considering both the upper and lower constraints on τ, this imposes an unsatisfactory choice of relaxation coefficients when the two domains have substantially different properties. For instance, for $D_2/D_1 = 0.001$, a selection of $\tau_1 = 2.5$ yields $\tau_2 = 0.502$, resulting in a very large τ_1 value and very small τ_2 that are close to the respective upper and lower limits.

III. PROPOSED MULTIPLE-TIME-SCALING LBM (MTS-LBM)

Our MTS strategy would allow one to choose the relaxation coefficients in different domains independently, to have both good numerical stability and accuracy. Moreover, as will be shown later in this section, MTS and the consistent interface treatment would enable one to model transport phenomena in adjacent domains separately in both space and time, i.e., the grid resolution, time steps, and modeling parameters in different domains can be decoupled from each other. This can greatly expand the modeling capability and efficiency of the LBM for multiphase and multicomponent flow and transport simulations.

For brevity, we assume that both domains have the same length-scaling factor. By introducing two independent time-scaling factors $L_t^{(1)}$ and $L_t^{(2)}$, the following is obtained:

$$\frac{2\tau_{2\lambda} - 1}{2\tau_1 - 1}\frac{L_t^{(1)}}{L_t^{(2)}} = \frac{D_2}{D_1}. \tag{4}$$

Denoting

$$L_t^{(2)} = L_t^{(1)}/\lambda \text{ and } D_{2\lambda} = D_2/\lambda, \tag{5}$$

we arrive at

$$\frac{2\tau_{2\lambda} - 1}{2\tau_1 - 1} = \frac{D_{2\lambda}}{D_1}. \tag{6}$$

Equation (6) implies that the thermal or mass diffusivity in the recovered CDE becomes $D_{2\lambda}$ when $\tau_{2\lambda}$ is used as the relaxation coefficient in the LB model. To preserve the solution to the original CDE, we rescale the CDE in Domain 2 by dividing each term by λ to yield

$$\partial_{t_\lambda}\phi_2 + \nabla \cdot (\mathbf{u}_{2\lambda}\phi_2) = \nabla \cdot (D_{2\lambda}\nabla\phi_2) + G_{2\lambda}, \tag{7a}$$

with

$$t_\lambda = \lambda t, \quad \mathbf{u}_{2\lambda} = \mathbf{u}_2/\lambda \text{ and } G_{2\lambda} = G_2/\lambda. \tag{7b}$$

And the conjugate flux condition at the interface should also be rescaled as

$$\Phi_{n1} = -\mathbf{n}_1 \cdot (D_1\nabla\phi_1 + \mathbf{u}_1\phi_1) = \mathbf{n}_2 \cdot \lambda(D_{2\lambda}\nabla\phi_2 + \mathbf{u}_{2\lambda}\phi_2) = -\lambda\Phi_{n,2\lambda}. \tag{8}$$

The comparison of the relations in Eqs. (3) and (6) shows that the relaxation coefficients τ_1 and $\tau_{2\lambda}$ can be chosen independently when two time-scaling factors are applied. In addition, rescaling of the flow velocity and source term in Domain 2 is required as shown in Eqs. (7a) and (7b). Recalling the upper limit of the magnitude of flow velocity in the LBM simulations [28], one needs to check the possible range of the rescaled velocity when choosing the two relaxation coefficients τ_1 and $\tau_{2\lambda}$ according to D_2/D_1 and λ.

The time rescaling in Eq. (7b), $t_\lambda = \lambda t$, can be understood in such a way—the simulation time step Δt_2 in Domain 2

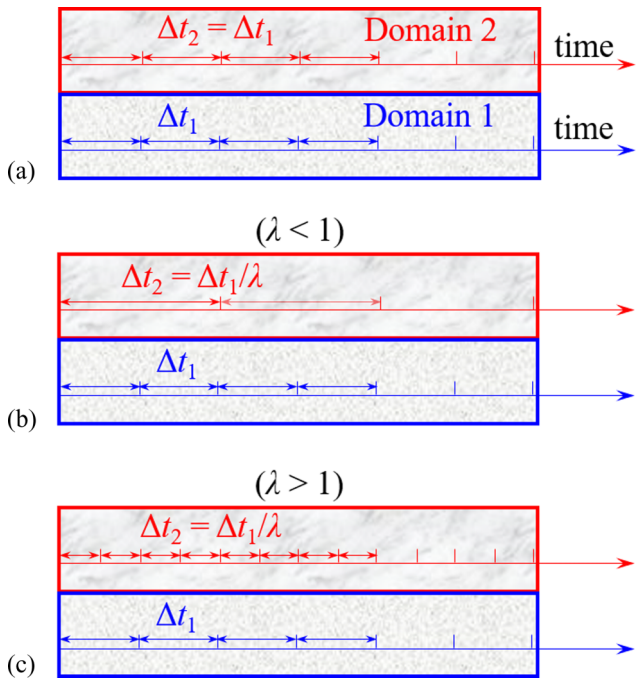

FIG. 1. Illustration of the multiple-time scaling (MTS) in LB simulations of transport between domains with different properties: (a) standard treatment (single-time scaling) with the same time step in both Domains 1 and 2, (b) MTS with $\lambda < 1$, i.e., time-step coarsening in Domain 2, and (c) MTS with $\lambda > 1$, i.e., time-step refinement in Domain 2. Note that the time steps in each domain can be "stretched" and λ does not have to be constant; see Fig. 15 for details.

is related to the original, i.e., not rescaled, time step Δt_1 in Domain 1 as

$$\Delta t_2 = \Delta t_1/\lambda. \tag{9}$$

A schematic is shown in Fig. 1 to illustrate the MTS strategy.

The key in the MTS strategy is the guarantee of interface conditions (i.e., continuity of or jumps in the scalar and its fluxes at the interface [11,29]) for unsteady simulations without nested iterations in each time step.

The interface treatment in the LBM computations should also be modified due to the rescaling. This can be conveniently handled when applying the 2nd-order accurate interface scheme by Li *et al.* [11]. We present below the modified interface scheme for parallel straight interfaces located "halfway" between lattice nodes (i.e., $\Delta = |(\mathbf{x}_{\rm int} - \mathbf{x}_1)/(\mathbf{x}_2 - \mathbf{x}_1)| = 0.5$),

$$g_{\bar\alpha}(\mathbf{x}_1, t + \Delta t_1) = \left(\frac{1-\lambda}{1+\lambda}\right)\hat g_\alpha(\mathbf{x}_1, t) + \left(\frac{2\lambda}{1+\lambda}\right)\hat g_{\bar\alpha}(\mathbf{x}_2, t), \quad (\Delta = 0.5), \tag{10a}$$

$$g_\alpha(\mathbf{x}_2, t + \Delta t_2) = -\left(\frac{1-\lambda}{1+\lambda}\right)\hat g_{\bar\alpha}(\mathbf{x}_2, t) + \left(\frac{2}{1+\lambda}\right)\hat g_\alpha(\mathbf{x}_1, t), \quad (\Delta = 0.5), \tag{10b}$$

where $\mathbf{e}_{\bar\alpha} = -\mathbf{e}_\alpha$, $\mathbf{x}_1$ and $\mathbf{x}_2$ are on the lattice nodes adjacent to the interface ($\mathbf{x}_{\rm int}$), and $\hat g$ represents the postcollision distribution function. The interface treatment in Eq. (10) is able to preserve the conjugate conditions up to 2nd-order accuracy in space. The interpolation-based interface schemes for general intersection Δ values and for curved geometry can be similarly obtained.

Implementation of the proposed multiple-time scaling (MTS) in different domains is straightforward and convenient. For time-step coarsening in Domain 2 ($\lambda < 1$, $\Delta t_2 = \Delta t_1/\lambda$), the explicit time marching in Domain 2 is executed once for every $1/\lambda$ time steps in Domain 1. Within this time window, update of the distribution functions (DFs) is conducted only for Domain 1. And the same postcollision DFs, $\hat g_{\bar\alpha}(\mathbf{x}_2, t)$, in the lattice nodes within Domain 2 and next to the interface, are utilized for the interface treatment for Domain 1. On the contrary, for time-step refinement in Domain 2 ($\lambda > 1$), the DFs in Domain 2 are updated λ times within each time step Δt_1 of Domain 1. The time-dependent boundary condition and source term can be exactly updated within each step of Δt_2 or remain the same within the steps of $\Delta t_1 = \lambda \Delta t_2$. Our numerical results show that their difference is very small (see discussion about Fig. 18 below). In the LBM implementations, the time step is usually chosen as unity in the LB unit, i.e., $\delta_t = 1$. Therefore, in order to match the solutions of ϕ_1 and ϕ_2 in the two domains at the exact same physical time, one would choose λ and $1/\lambda$ as integers in time-step refinement and coarsening, respectively. It should also be noted that the time steps in each domain can be "stretched" and λ does not have to be constant (as demonstrated in Fig. 15 below).

The combination of MTS and the interface treatment enables one to model the transport phenomena in the two adjacent domains separately in both space and time, while preserving the conjugate conditions at the interface without any iterations (i.e., the interface conditions are satisfied within

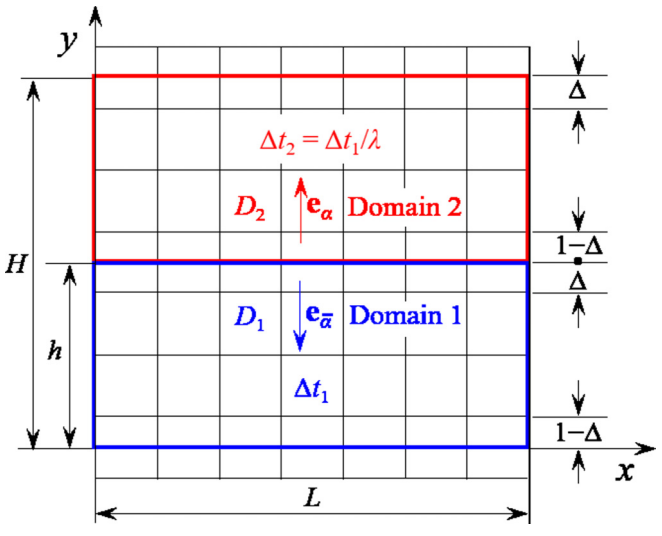

FIG. 2. Schematic depiction of the computational domain for the convection diffusion in a channel with multiple-time scaling, $\Delta t_2 = \Delta t_1/\lambda$, in the two domains.

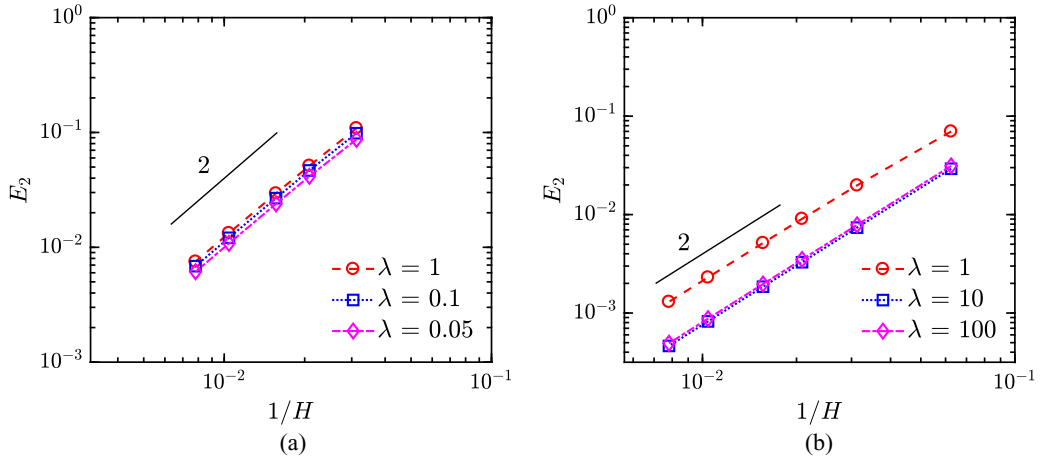

FIG. 3. Relative L_2-norm error E_2 for the interior field of ϕ vs the grid resolution $1/H$ for steady convection diffusion (Pe $= 20$) in the 2D channel with (a) $D_2/D_1 = 0.05$ and (b) $D_2/D_1 = 100$. A line with slope $= 2$ is shown in each plot.

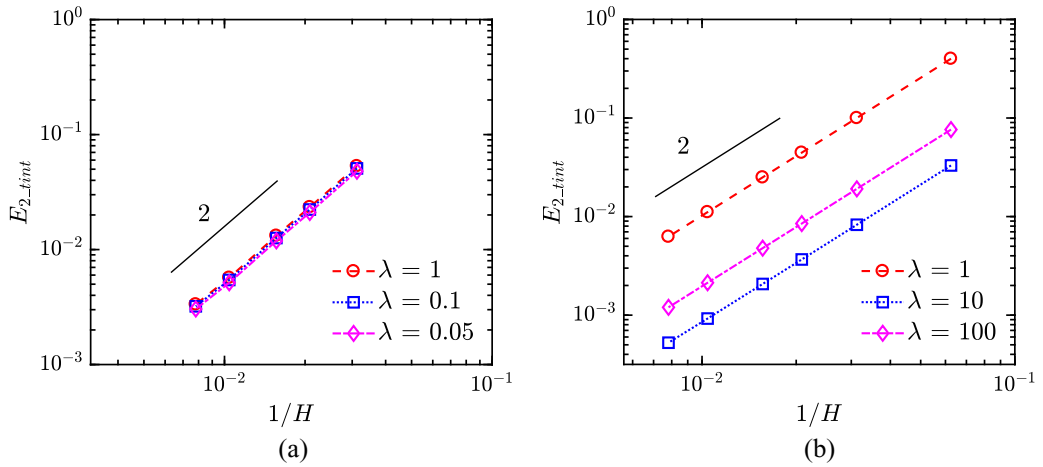

FIG. 4. Relative L_2-norm error E_{2_tint} for the interfacial ϕ values vs $1/H$ for steady convection diffusion (Pe $= 20$) in the channel with (a) $D_2/D_1 = 0.05$ and (b) $D_2/D_1 = 100$.

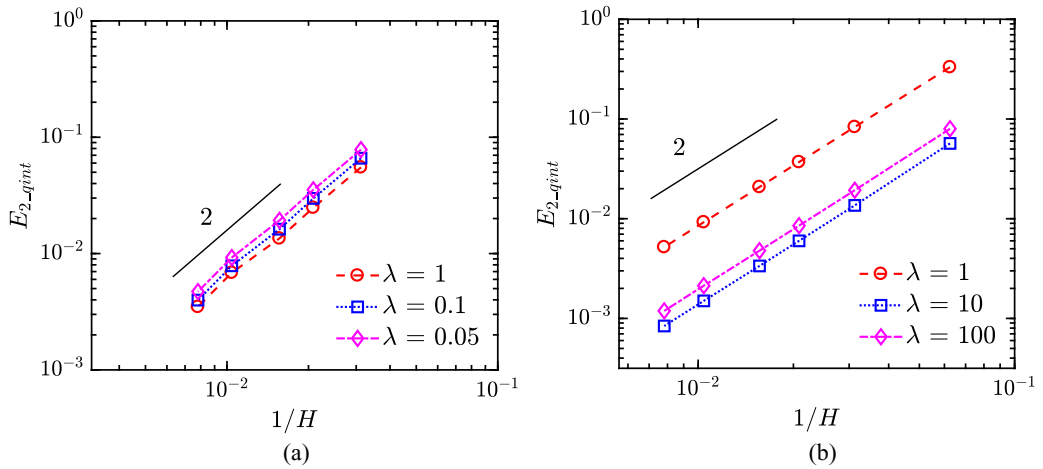

FIG. 5. Relative L_2-norm error E_{2_qint} for the interfacial fluxes vs $1/H$ for steady convection diffusion (Pe $= 20$) in the channel with (a) $D_2/D_1 = 0.05$ and (b) $D_2/D_1 = 100$.

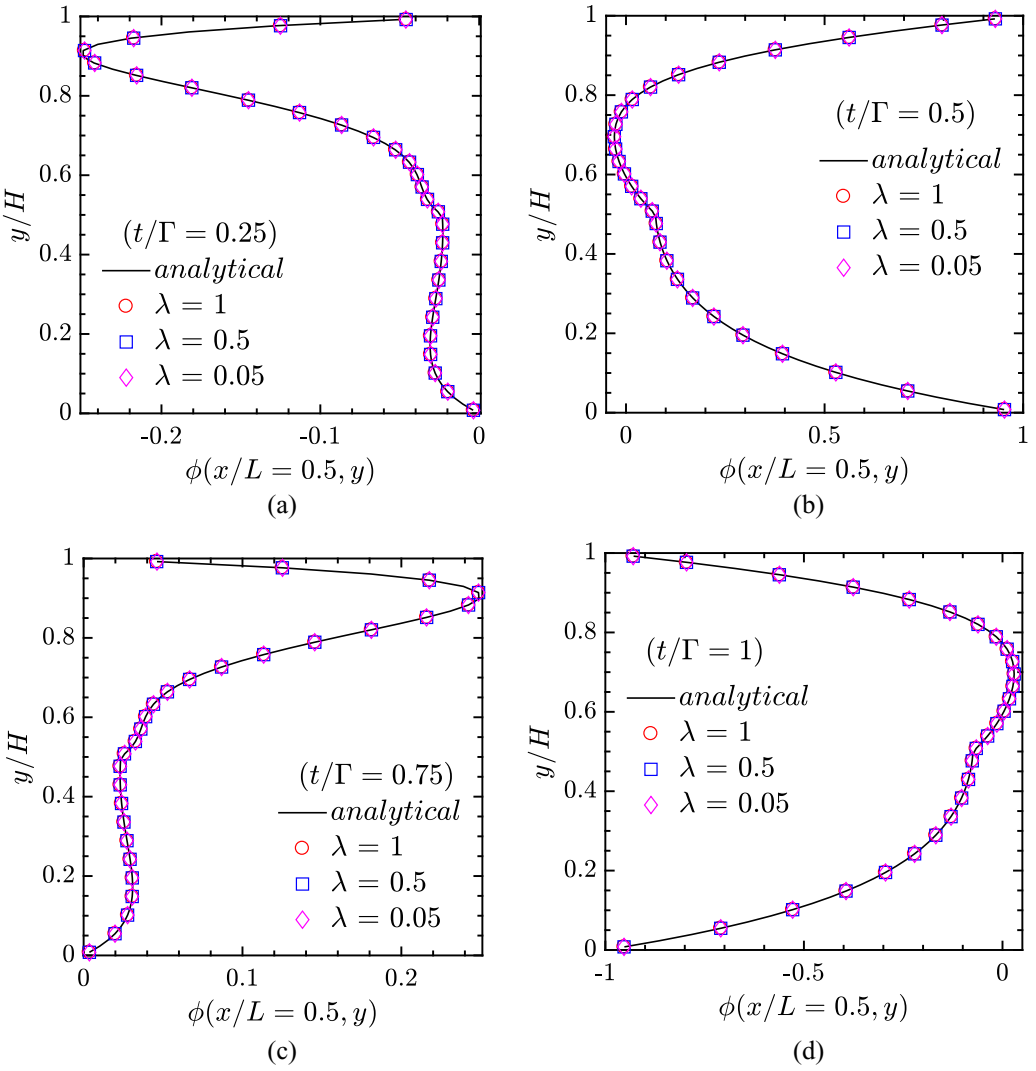

FIG. 6. Comparison between the LBM and analytical solutions for the scalar profile $\phi(x/L = 0.5)$ at (a) $t/\Gamma = 0.25$, (b) $t/\Gamma = 0.5$, (c) $t/\Gamma = 0.75$, and (d) $t/\Gamma = 1.0$ for pure diffusion (Pe = 0).

each time step). As a consequence, the grid resolution, time steps, and modeling parameters in different domains are decoupled from each other. This is an extremely valuable feature for the LBM to be applied to optimize the simulations in different domains and to be able to simulate transport between domains with large property ratios.

Furthermore, the present MTS strategy preserves the explicitness of the LBM and enhances the compatibility with parallelization as the different domains are decoupled in both spatial and temporal evolutions with simple information transfer at the interface. It is thus envisioned that the MTS strategy would greatly broaden the applications of LBM, especially for systems with multicomponents and multiphases.

Lastly, while the emphasis is placed on MTS for transient problems, the decoupling of the relaxation coefficients in different domains [see Eq. (6)] with the modified interface treatment in Eq. (10) is directly applicable to steady-state simulations. This is also verified in the numerical examples in Sec. IV.

IV. NUMERICAL TESTS AND DISCUSSION

We demonstrate the applicability and accuracy of the MTS strategy in the LBM with two numerical tests for which analytical solutions are available. The multiple-relaxation-time (MRT) LB model with a D2Q5 lattice [16,17] is applied for the CDE.

A. Convection diffusion in a 2D channel filled with two fluids

The first test is for convection diffusion in a two-dimensional (2D) channel filled with two fluids. This test was designed in [11] and has been widely applied for evaluating various interface schemes proposed in the LBM for conjugate heat and mass transfer simulations. For completeness, the schematic of the computational domain is shown in Fig. 2. Following [11], a constant plug flow $\mathbf{u} = (U, 0)$ is assumed for both domains. The steady-state case is first used to verify the decoupling of the relaxation coefficients in the two domains and the modified interface treatment; afterwards,

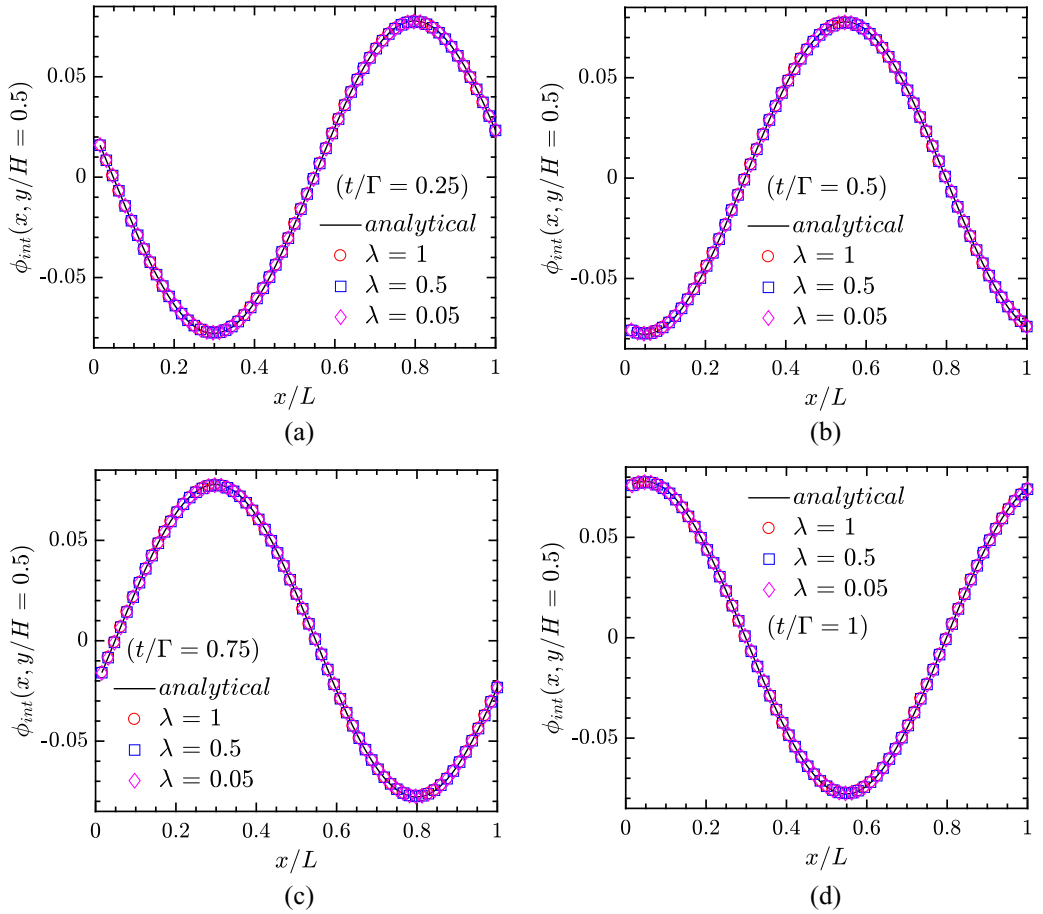

FIG. 7. Comparison between the LBM and analytical solutions for the interfacial scalar at (a) $t/\Gamma = 0.25$, (b) $t/\Gamma = 0.5$, (c) $t/\Gamma = 0.75$, and (d) $t/\Gamma = 1.0$ for pure diffusion (Pe = 0).

the applicability and accuracy of the MTS strategy for unsteady convection diffusion is scrutinized. For the general unsteady situation, a sinusoidal boundary condition in both space and time is specified on the walls with $\phi_w(t, x, y = 0) = \phi_w(t, x, y = H) = \cos[2\pi(x/L + t/\Gamma)]$, where Γ is the period. The analytical solutions for both steady and unsteady cases can be found in [11]. For brevity, we consider only the situation with the boundaries and interface located halfway between lattice nodes (intersection link fractions all with $\Delta = 0.5$ in Fig. 2).

To check the numerical accuracy and convergence order, the following time-averaged L_2-norm errors are defined:

$$E_2 = \left\{ \frac{1}{\Gamma} \int_0^{\Gamma} \left[\sum_{x,y} (\phi_{\mathrm{LBE}} - \phi_{\mathrm{ex}})^2 \Big/ \sum_{x,y} \phi_{\mathrm{ex}}^2 \right] dt \right\}^{1/2}, \tag{11}$$

$$E_{2\_\mathrm{tint}} = \left\{ \frac{1}{\Gamma} \int_0^{\Gamma} \left[\sum_{x,y=h} (\phi_{1,2}|_{\mathrm{LBE}} - \phi_{1,2}|_{\mathrm{ex}})^2 \Big/ \sum_{x,y=h} (\phi_{1,2}|_{\mathrm{ex}})^2 \right] dt \right\}^{1/2}, \tag{12}$$

$$E_{2\_\mathrm{qint}} = \left\{ \frac{1}{\Gamma} \int_0^{\Gamma} \left[\sum_{x,y=h} \left(D_{1,2} \frac{\partial \phi_{1,2}}{\partial y}\Big|_{\mathrm{LBE}} - D_{1,2} \frac{\partial \phi_{1,2}}{\partial y}\Big|_{\mathrm{ex}} \right)^2 \Big/ \sum_{x,y=h} \left(D_{1,2} \frac{\partial \phi_{1,2}}{\partial y}\Big|_{\mathrm{ex}} \right)^2 \right] dt \right\}^{1/2}, \tag{13}$$

where E_2 contains the relative errors at all the lattice nodes in the interior of both domains, and E_{2_tint} and E_{2_qint} evaluate the relative errors of the macroscopic value ϕ and its flux at the interface, respectively. The details for the calculation of the interfacial scalar and flux values can be found in [11]. For steady-state simulations, the

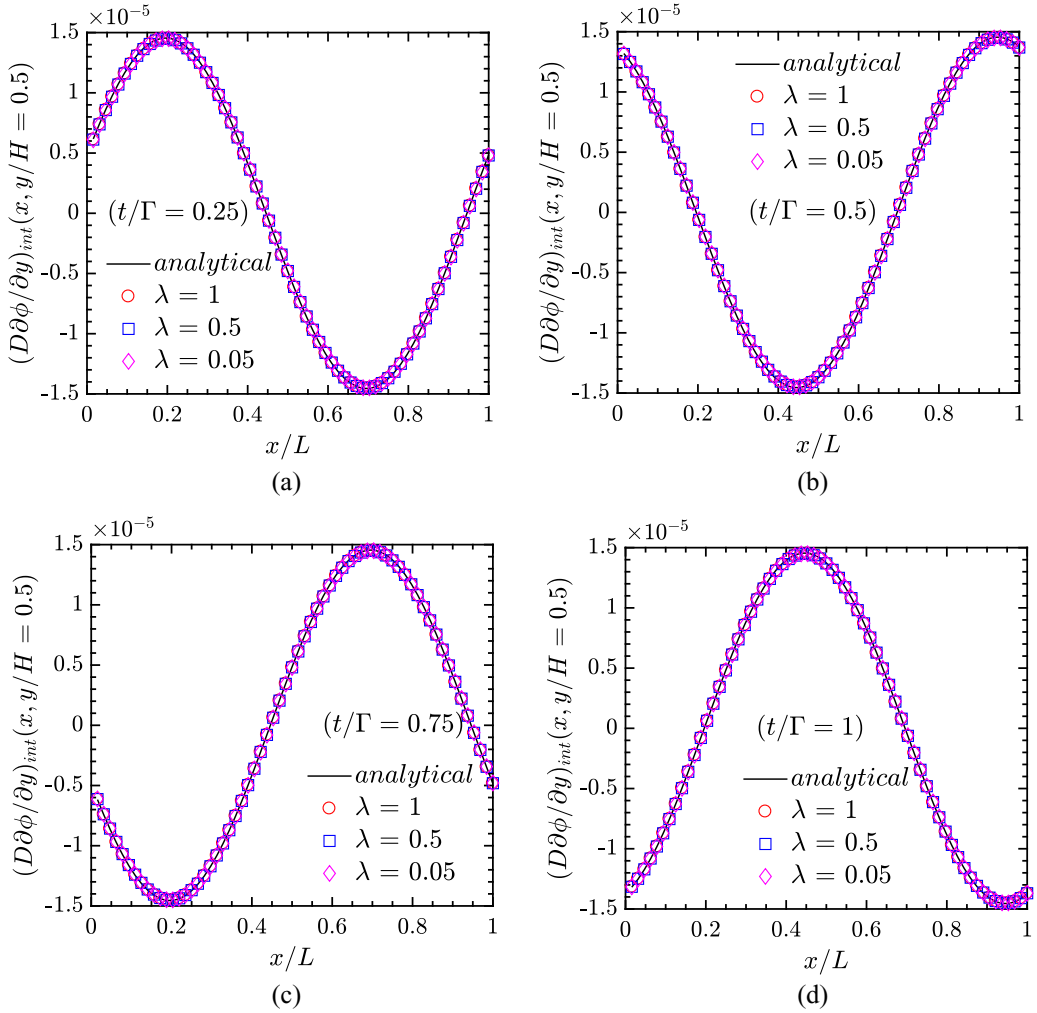

FIG. 8. Comparison between the LBM and analytical solutions for the interfacial flux at (a) $t/\Gamma = 0.25$, (b) $t/\Gamma = 0.5$, (c) $t/\Gamma = 0.75$, and (d) $t/\Gamma = 1.0$ for pure diffusion (Pe = 0).

definition of the L_2-norm errors is simplified without time averaging.

1. Steady-state convection diffusion in the channel

For each case shown below, we choose a fixed relaxation coefficient τ_1 for Domain 1; and τ_2 for Domain 2 is determined only by D_2/D_1 without MTS, or by D_2/D_1 and the parameter, λ, between the two time-scaling factors ($L_t^{(2)} = L_t^{(1)}/\lambda$) with MTS. It should be noted that for $\lambda \neq 1$, the interface treatment in Eq. (10) needs to be implemented.

Figures 3–5 show the respective relative L_2-norm errors for the interior scalar field, the interfacial scalar, and its fluxes. The characteristic Péclet number is at $\mathrm{Pe} = UH/D_1 = 20$. Two different cases with diffusivity ratios $D_2/D_1 = 0.05$ and $D_2/D_1 = 100$ for the two domains are considered with $\tau_1 = 0.55$ and $\tau_1 = 0.52$ used, respectively.

Second-order convergence is observed for all cases. Moreover, very close errors are noticed in part (a) of each figure for $D_2/D_1 = 0.05$, while in part (b) the error magnitude drops significantly from $\lambda = 1$ to $\lambda = 10$, 100. This is due to the error dependence on the relaxation parameters used in the LBM ($\tau_{2\lambda} = 2.5$, 0.7, and 0.51 with $\lambda = 1$, 10, and 100, respectively), as also observed in previous works [16,25–27]. This steady-state test confirms the second-order accuracy of the modified interface treatment in Eq. (10) for decoupling of the relaxation coefficients in different domains.

2. Unsteady convection diffusion in the channel

The unsteady case with pure diffusion (Pe = 0) is considered first to verify the MTS strategy. A fixed relation coefficient $\tau_1 = 0.55$ is chosen and $\tau_{2\lambda}$ is selected according to the scaling factor λ as in Eq. (6). With MTS, the time step in Domain 2 is related to that in Domain 1 as $\Delta t_2 = \Delta t_1/\lambda$. The characteristic Stokes number is chosen as $\mathrm{St} = \sqrt{\frac{H^2}{\Gamma D_1}} = 1$. Comparison of the LBM profiles for the scalar at $x/L = 0.5$ and the interfacial scalar value and its fluxes at different times, $t/\Gamma = 0.25$, 0.5, 0.75 and 1.0, with analytical solutions for $D_2/D_1 = 0.05$ and $H = 64\Delta x$ is plotted in Figs. 6–8, respectively. Excellent agreement with analytical solutions is observed for all cases. The same is observed for the cases with time-step refinement in Domain 2 ($\lambda = 1$, 10, and 50 used for $D_2/D_1 = 50$) and not shown here for brevity.

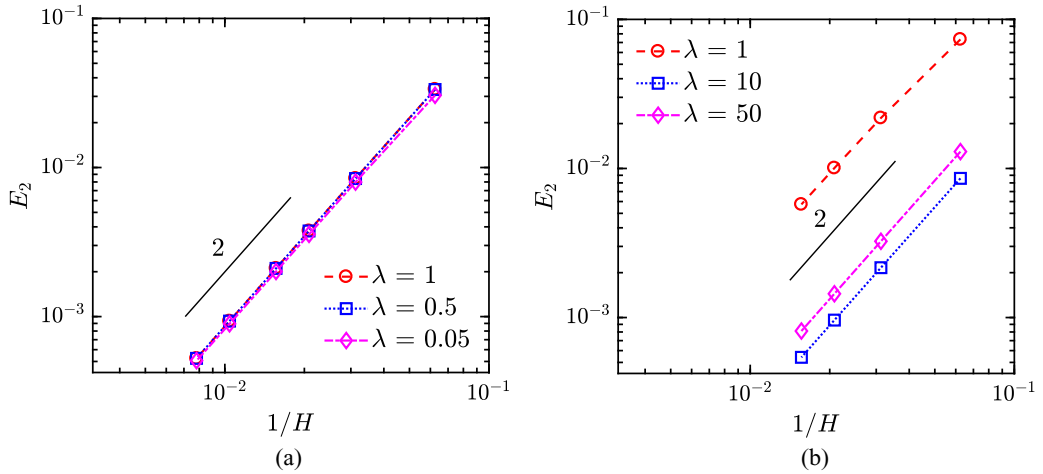

FIG. 9. Time-averaged relative L_2-norm error E_2 for the interior field of ϕ vs $1/H$ for unsteady diffusion (Pe $= 0$) in the 2D channel with (a) $D_2/D_1 = 0.05$ and (b) $D_2/D_1 = 50$.

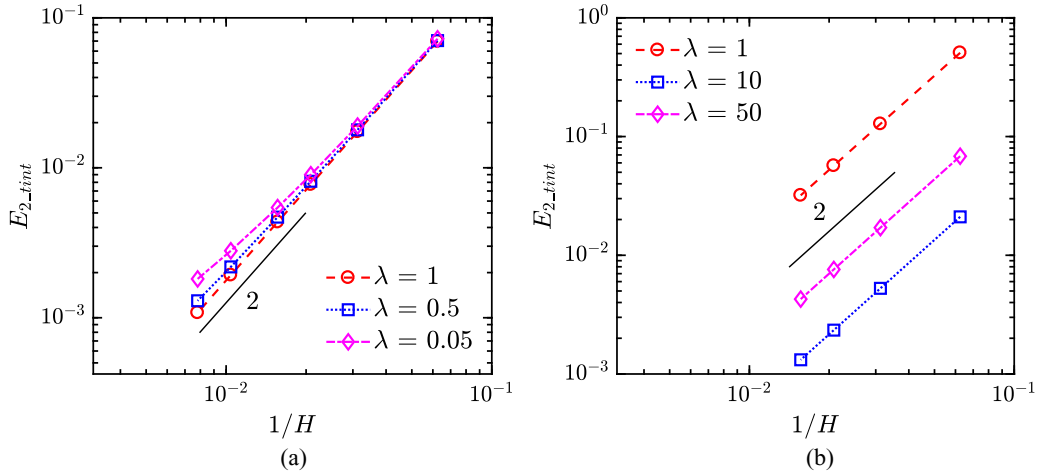

FIG. 10. Time-averaged relative L_2-norm error E_{2_tint} for the interfacial ϕ values vs $1/H$ for unsteady diffusion (Pe $= 0$) in the channel with (a) $D_2/D_1 = 0.05$ and (b) $D_2/D_1 = 50$.

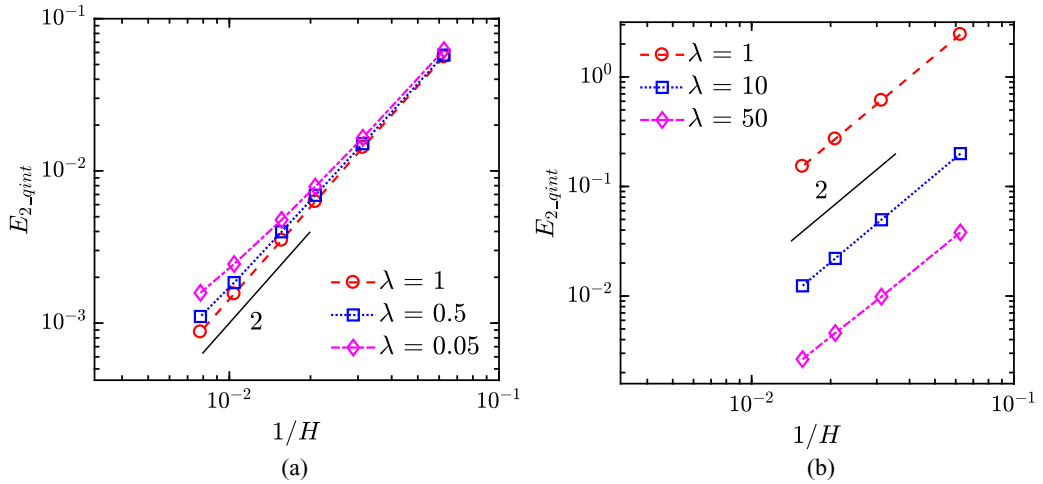

FIG. 11. Time-averaged relative L_2-norm error E_{2_qint} for the interfacial fluxes vs $1/H$ for unsteady diffusion (Pe $= 0$) in the channel with (a) $D_2/D_1 = 0.05$ and (b) $D_2/D_1 = 50$.

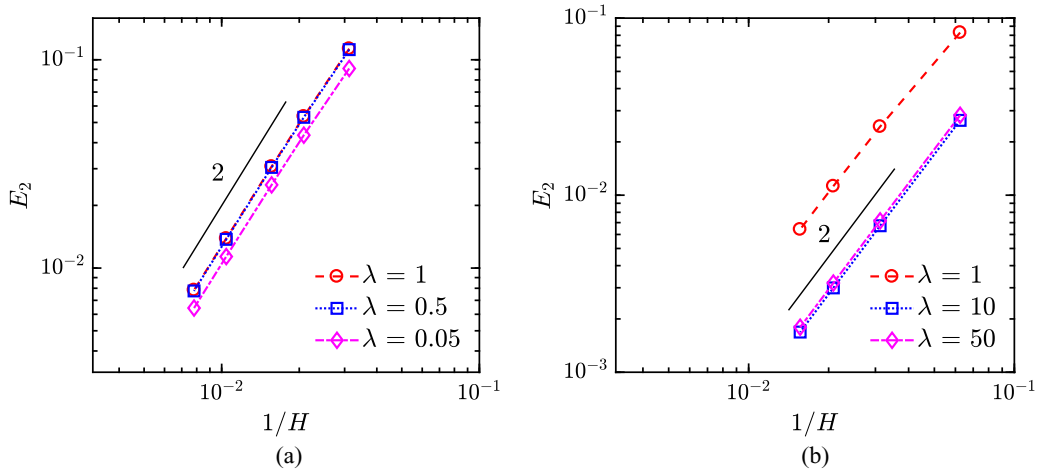

FIG. 12. Time-averaged relative L_2-norm error E_2 for the interior field of ϕ vs $1/H$ for unsteady convection diffusion (Pe = 20) in the channel with (a) $D_2/D_1 = 0.05$ and (b) $D_2/D_1 = 50$.

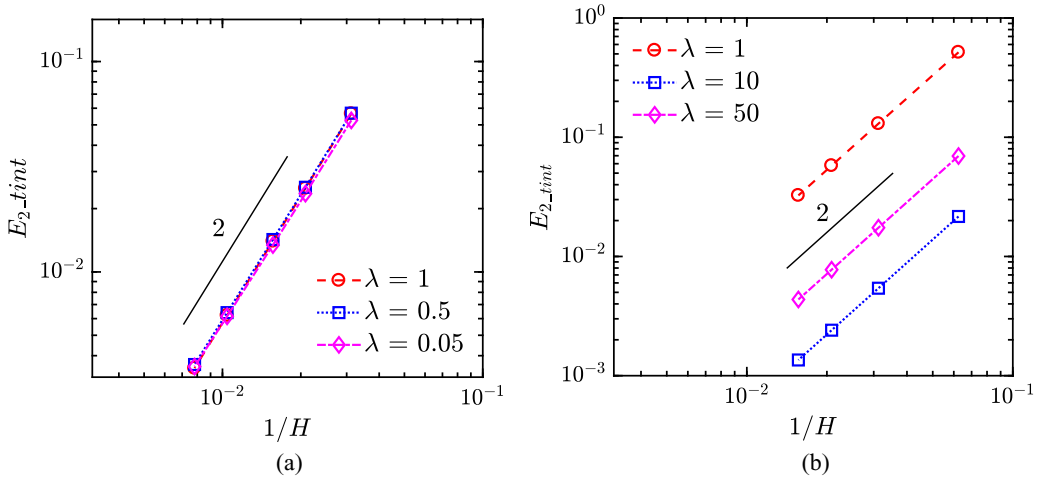

FIG. 13. Time-averaged relative L_2-norm error E_{2_tint} for the interfacial ϕ values vs $1/H$ for unsteady convection diffusion (Pe = 20) in the channel with (a) $D_2/D_1 = 0.05$ and (b) $D_2/D_1 = 50$.

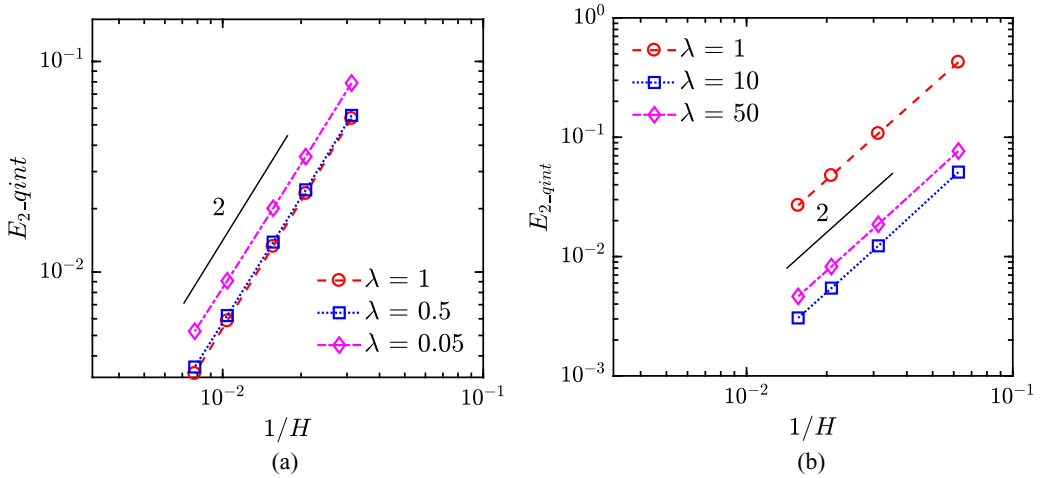

FIG. 14. Time-averaged relative L_2-norm error E_{2_qint} for the interfacial fluxes vs $1/H$ for unsteady convection diffusion (Pe = 20) in the channel with (a) $D_2/D_1 = 0.05$ and (b) $D_2/D_1 = 50$.

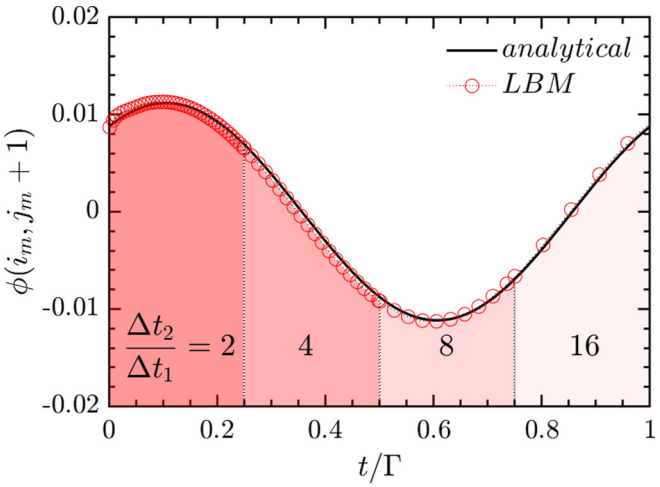

FIG. 15. Comparison between the LBM and analytical solutions for the scalar value with continuously changing (stretched) time steps in Domain 2.

The time-averaged L_2-norm errors defined in Eqs. (11)–(13) for the three quantities of interest are shown in Figs. 9–11. For time-step refinement ($\lambda > 1$), second-order convergence is obtained for all cases, and the error magnitude is substantially reduced compared to the baseline case without MTS ($\lambda = 1$). For time-step coarsening ($\lambda < 1$), second-order convergence is preserved for the interior field of ϕ, while for the interfacial scalar value and flux, slightly larger error magnitude and deviation from the 2nd-order convergence is noticed at high grid resolution, owing to the larger time steps used in Domain 2. Overall, the applicability and accuracy of the MTS strategy for transient diffusion is verified.

Next, general unsteady convection and diffusion in the channel is considered and the velocity rescaling [see Eq. (7b)] was conducted within MTS. Figures 12–14 show the results of time-averaged relative L_2-norm errors at Pe = 20 and St = 1. Again, fixed $\tau_1 = 0.55$ is chosen and $\tau_{2\lambda}$ is selected according to λ; and the time step in Domain 2 is $\Delta t_2 = \Delta t_1/\lambda$, noting that the velocity in Domain 2 is also rescaled. Second-order accuracy is obtained for all cases. The error increase and convergence order deviation in Figs. 10(a) and 11(a) are not noticed here, as the overall error magnitude is higher with the convection effect, and hence the error caused by the time-step enlargement, which is of the order of 10^{-3}, is not seen in Figs. 13 and 14. This demonstrates the applicability and accuracy of the proposed MTS strategy for general unsteady convection diffusion with both types of time-step coarsening and refinement.

As a further step, we demonstrate the accuracy of the MTS strategy for continuously varying time steps, i.e., with the time step *stretched* in Domain 2. Figure 15 shows the transient LBM result for the scalar $\phi(i_m, j_m + 1)$ at the lattice node next to the interface [the coordinates for that node are ($x/L = 0.5$, $y/H = 0.5(1 + \Delta x/H)$, with Δx the uniform grid size]. The parameters used are $D_2/D_1 = 0.05$, Pe = 20, St = 1, $H = 64\Delta x$, and $\tau_1 = 0.625$. The time step in Domain 2 is twice that in Domain 1 ($\Delta t_2 = \Delta t_1/\lambda = 2\Delta t_1$) during the first quarter of the period Γ; and it was doubled in each of the next three quarters. It is highlighted that straightforward and consecutive time marching was performed throughout the entire period, and there was no need for iteration when an abrupt change in the time step was encountered. Excellent agreement is seen in Fig. 15 between the LBM and analytical solutions for the entire period. Probe of the LBM results at other nodes in the two domains was also conducted and the same conclusion holds. This confirms the applicability, accuracy, and ease in implementation of the proposed MTS strategy.

B. Womersley flow in a 2D channel with immiscible fluids

To further investigate the rescaling of the source term and the temporal accuracy of the MTS approach, we present next the results for the Womersley flow [30,31] in a 2D channel with two-layered immiscible fluids. An oscillating pressure gradient, $dP/dx = \mathrm{Re}[Ae^{i\omega t}]$, is imposed and the flow is

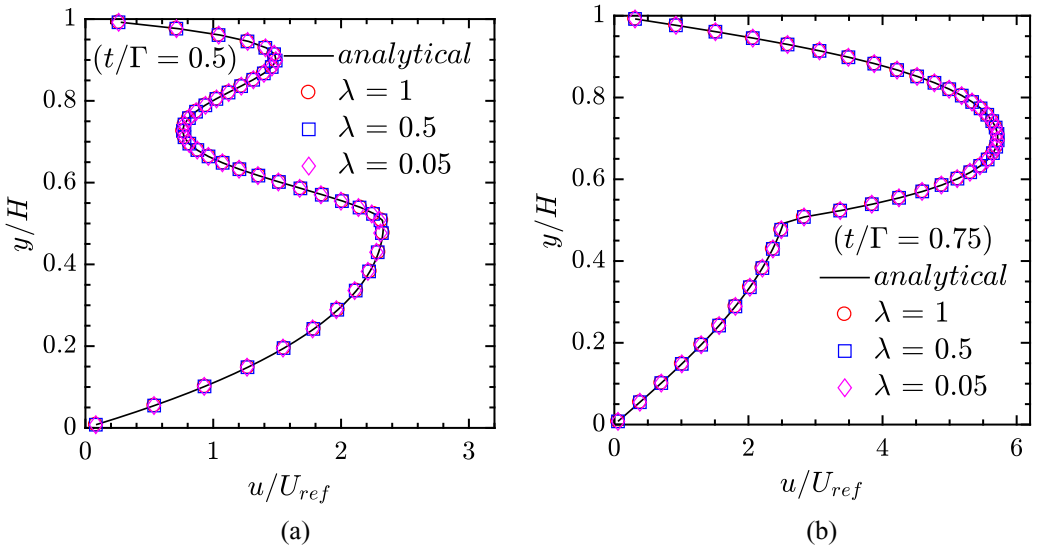

FIG. 16. Comparison between the LBM and analytical solutions for the velocity profile at (a) $t/\Gamma = 0.5$ and (b) $t/\Gamma = 0.75$ for $D_2/D_1 = 0.05$.

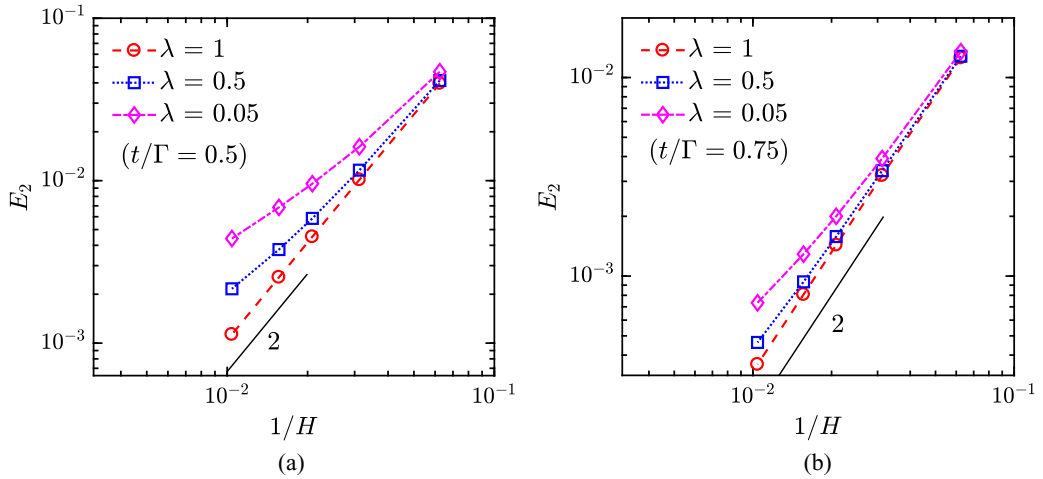

FIG. 17. Instant relative L_2-norm error for the interior velocity field vs $1/H$ at (a) $t/\Gamma = 0.5$ and (b) $t/\Gamma = 0.75$ for $D_2/D_1 = 0.05$.

assumed to be laminar and fully developed. We treat $u(t, y)$ as a scalar and its governing equation a CDE (the diffusion coefficients are set to be equal to the viscosities $D_{1,2} = \upsilon_{1,2}$) with the pressure gradient a transient source term. Following [30], the analytical solution can be obtained with no-slip wall boundary conditions and velocity and shear stress continuity interface conditions:

$$u_1(t, y) = \mathrm{Re}\left\{e^{i\omega t}\left[i\frac{A}{\omega} + c_{11}\cos(\beta_1 y) + c_{12}\sin(\beta_1 y)\right]\right\}, \tag{14}$$

$$u_2(t, y) = \mathrm{Re}\left\{e^{i\omega t}\left[i\frac{A}{\omega} + c_{21}\cos(\beta_2 y) + c_{22}\sin(\beta_2 y)\right]\right\}, \tag{15}$$

where $\beta_{1,2} = \sqrt{\frac{-i\omega}{\upsilon_{1,2}}}$ and $c_{11} = -i\frac{A}{\omega}$, $c_{12} = \frac{B_1C_2 - B_2C_1}{A_2B_1 - A_1B_2}$, $c_{21} = -\frac{\sin(\beta_2 H)}{\cos(\beta_2 H)}\frac{A_2C_1 - A_1C_2}{A_2B_1 - A_1B_2} - \frac{iA}{\omega\cos(\beta_2 H)}$, $c_{22} = \frac{A_2C_1 - A_1C_2}{A_2B_1 - A_1B_2}$, with $A_1 = \sin(\beta_1 h)$, $A_2 = \beta_1\cos(\beta_1 h)$, $B_1 = \frac{\sin[\beta_2(H-h)]}{\cos(\beta_2 H)}$, $B_2 = -\frac{\upsilon_2}{\upsilon_1}\frac{\beta_2\cos[\beta_2(H-h)]}{\cos(\beta_2 H)}$, $C_1 = i\frac{A}{\omega}[\cos(\beta_1 h) - \frac{\cos(\beta_2 h)}{\cos(\beta_2 H)}]$, and $C_2 = i\frac{A}{\omega}[\frac{\upsilon_2}{\upsilon_1}\frac{\beta_2\sin(\beta_2 h)}{\cos(\beta_2 H)} - \beta_1\sin(\beta_1 h)]$.

Again, two different cases $D_2/D_1 = 0.05$ and $D_2/D_1 = 50$ are considered and the MTS approach is implemented for those cases with time-step coarsening ($\lambda < 1$) and refinement ($\lambda > 1$) in Domain 2, respectively. The simulation parameters include the Womersley number $Wo = \sqrt{\frac{H^2\pi}{2\Gamma D_1}} = \sqrt{\frac{\pi}{2}}$, Reynolds number $\mathrm{Re} = \frac{U_{\mathrm{ref}}H}{D_1} = 14\,745$, with $U_{\mathrm{ref}} = \frac{AH^2}{8D_1}$, and τ_1 is fixed at 0.55. The comparison between the instant LBM and analytical solutions was checked first (the simulations were conducted for several periods). Excellent agreement was observed at all times, and Fig. 16 shows representative results at two instants for selected λ values (the interface is placed at $y = h = H/2$).

In addition, Figs. 17 and 18 show the relative L_2-norm errors at selected times with both time-step coarsening ($\lambda < 1$) and refinement ($\lambda < 1$). And the time-averaged relative L_2-norm errors are summarized in Fig. 19. Consistent with the results in the previous example, second-order accuracy is preserved for $\lambda \geqslant 1$, and the convergence deviates from the second order at high grid resolution for $\lambda < 1$. This deviation (error increase with smaller λ) in Figs. 17 and 19(a) is due to the coarsened time steps used in Domain 2. To scrutinize the temporal errors, Figs. 20(a) and 20(b) show the relative error history for both situations for $H = 64\Delta x$. It becomes clear that with the selected parameters, time-step refinement in the half domain has a negligible effect on the global error reduction (error is mainly controlled by that in the other domain); while time-step coarsening increases the overall errors. The behavior of the convergence order deviation for the interior scalar field was not observed in the previous test in Fig. 9(a) or 12(a), while similar behavior was seen for the relative errors for the computed interfacial scalar and fluxes at $\mathrm{Pe} = 0$ [see Figs. 10(a) and 11(a)].

It should be emphasized that while the convergence deviates from the second order at high grid resolution with time-step coarsening, the relative error magnitude is rather small; and at low grid resolution, very close error magnitude is noticed for coarsened time steps compared to that with $\lambda = 1$. Moreover, with coarsened time steps, the computational cost is significantly reduced (20 times less with $\lambda = 0.05$

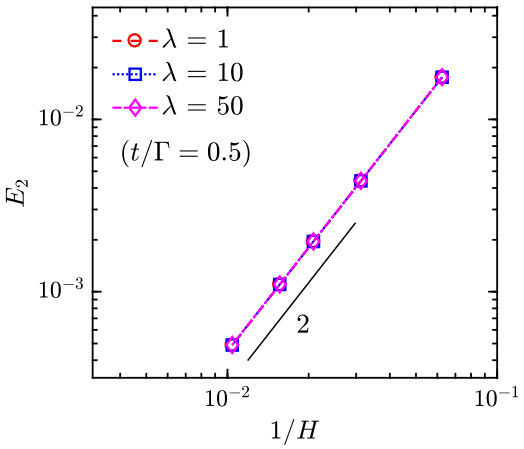

FIG. 18. Instant relative L_2-norm error for the interior velocity field vs $1/H$ at $t/\Gamma = 0.5$ for $D_2/D_1 = 50$.

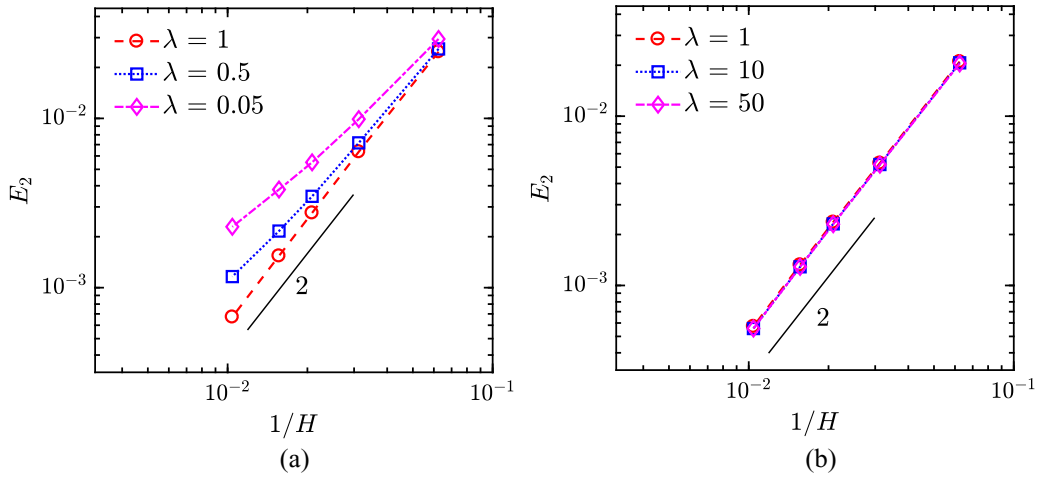

FIG. 19. Time-averaged relative L_2-norm error E_2 for the interior velocity field vs $1/H$ with (a) time-step coarsening in Domain 2 for $D_2/D_1 = 0.05$ and (b) time-step refinement in Domain 2 for $D_2/D_1 = 50$.

in Domain 2). This makes the proposed MTS an extremely attractive approach for large-scale computations.

We also compared the difference for the two types of implementation of the time-dependent source term when MTS was applied for time-step refinement. In the first type, the source term was updated for each step of refined Δt_2; while in the second type, it was only updated for each larger step $\Delta t_1 = \lambda \Delta t_2$. The data shown in Fig. 18 are for the latter, and the results for the former are very close and thus not repeated. It is hence recommended to use the first type of implementation to reduce computational cost, and the second type can be applied when rapid changes are encountered or expected.

V. CONCLUSIONS

We have proposed and demonstrated the multiple-time-scaling (MTS) strategy in the lattice Boltzmann method (LBM) to decouple the time discretization in different domains. The basic idea and implementation of the MTS-LBM is remarkably simple and straightforward. It enables independent time-step refinement, coarsening, and stretching in LBM modeling. The present MTS strategy preserves the explicitness of the LBM formulation and the locality in implementation, and enhances the compatibility with parallelization as the different domains are decoupled in both spatial and temporal evolutions with simple information transfer at the interface. Our method fills the gap of adjustable time scaling and discretization in the LBM development and application, and thus shows promise to extend the LBM as an effective and efficient numerical solver for complex multiphase and multicomponent flow and transport problems. For example, those phenomena between different materials and phases with large property ratios can be conveniently modeled with the MTS-LBM approach. The overall computational cost could be substantially reduced for large systems involving both rapid and slow evolutions by choosing suitable time steps for each spatial domain and time period. True parallelization in both space and time is envisioned in the LBM computations with the decoupling in both spatial and temporal scaling and discretization.

Here we used the LB model for the convection diffusion equation (CDE) to formulate the MTS strategy. A natural extension is to apply MTS to LB models for fluid flows and coupled thermo-chemical-hydrodynamic transport problems. However, this might not be as straightforward as that in the MTS-LBM approach for the CDE considering the nonlinear convection term in the Navier-Stokes equations and the re-

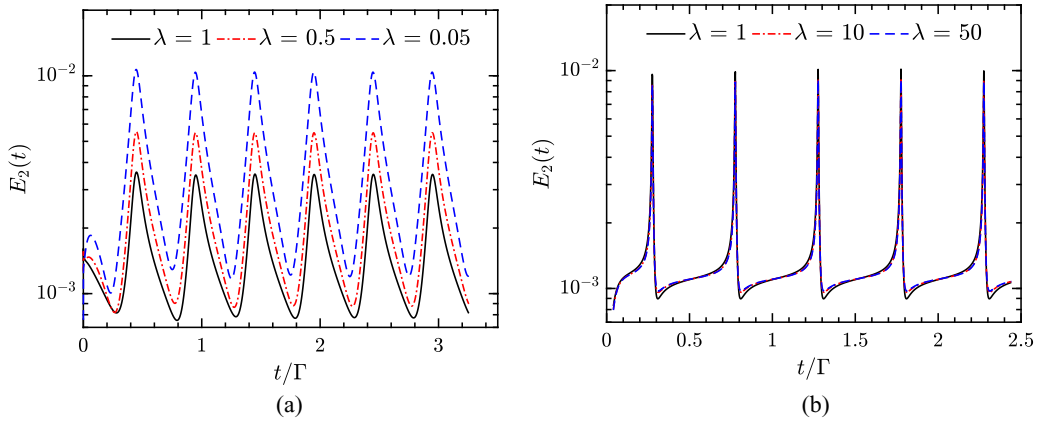

FIG. 20. Temporal variations of the instant relative L_2-norm error $E_2(t)$ for the 2D unsteady Womersley flow with (a) time-step coarsening, and (b) time-step refinement, as in Fig. 19.

quirement for effective interface schemes in LBM for fluid flows. Another remark is regarding the application of the MTS strategy for time-varying or moving interfaces such as those in [3]. While the idea of the MTS strategy is still applicable for such interfaces, the time steps in each domain adjacent to the interface should be much less than that used to track the interface variations or movement. Moreover, when there are new fluid nodes created and/or old fluid nodes destroyed (such as those with moving particles or particle deformation), modifications to the original interface treatment for conjugate conditions in [11] as well as to the present MTS strategy are required. These will be the objectives of future work.

ACKNOWLEDGMENT

The author acknowledges support from the Start-up Fund at Mississippi State University.

[1] D. A. Drew, Mathematical modeling of two-phase flow, Annu. Rev. Fluid Mech. **15**, 261 (1983).
[2] J. Sethian and P. Smereka, Level set methods for fluid interfaces, Annu. Rev. Fluid Mech. **35**, 341 (2003).
[3] Y. Sui, H. Ding, and P. Spelt, Numerical simulations of flows with moving contact lines, Annu. Rev. Fluid Mech. **46**, 97 (2014).
[4] A. Mazloomi M, S. S. Chikatamarla, and I. V. Karlin, Entropic Lattice Boltzmann Method for Multiphase Flows, Phys. Rev. Lett. **114**, 174502 (2015).
[5] M. Wohrwag, C. Semprebon, A. M. Moqaddam, I. Karlin, and H. Kusumaatmaja, Ternary Free-Energy Entropic Lattice Boltzmann Model with a High Density Ratio, Phys. Rev. Lett. **120**, 234501 (2018).
[6] R. Noriega, J. Rivnay, K. Vandewal, F. P. V. Koch, N. Stingelin, P. Smith, M. F. Toney, and A. Salleo, A general relationship between disorder, aggregation and charge transport in conjugated polymers, Nat. Mater. **12**, 1038 (2013).
[7] T. Mitchell, C. Leonardi, and A. Fakhari, Development of a three-dimensional phase-field lattice Boltzmann method for the study of immiscible fluids at high density ratios, Int. J. Multip. Flow **107**, 1 (2018).
[8] L. Fei, A. Scagliarini, A. Montessori, M. Lauricella, S. Succi, and K. H. Luo, Mesoscopic model for soft flowing systems with tunable viscosity ratio, Phys. Rev. Fluids **3**, 104304 (2018).
[9] M. L. Porter, E. T. Coon, Q. Kang, J. D. Moulton, and J. W. Carey, Multicomponent interparticle-potential lattice Boltzmann model for fluids with large viscosity ratios, Phys. Rev. E **86**, 036701 (2012).
[10] H. W. Zheng, C. Shu, and Y. T. Chew, A lattice Boltzmann model for multiphase flows with large density, J. Comput. Phys. **218**, 353 (2006).
[11] L. Li, C. Chen, R. Mei, and J. F. Klausner, Conjugate heat and mass transfer in the lattice Boltzmann equation method, Phys. Rev. E **89**, 043308 (2014).
[12] C. L. Lin and Y. G. Lai, Lattice Boltzmann method on composite grids, Phys. Rev. E **62**, 2219 (2000).
[13] S. Succi, *The Lattice Boltzmann Equation for Fluid Dynamics and Beyond* (Oxford University Press, Oxford, 2001).
[14] S. Chen and G. D. Doolen, Lattice Boltzmann method for fluid flows, Annu. Rev. Fluid Mech. **30**, 329 (1998).
[15] C. K. Aidun and J. R. Clausen, Lattice-Boltzmann method for complex flows, Annu. Rev. Fluid Mech. **42**, 439 (2010).
[16] H. Yoshida and M. Nagaoka, Multiple-relaxation-time lattice Boltzmann model for the convection and anisotropic diffusion equation, J. Comput. Phys. **229**, 7774 (2010).
[17] L. Li, R. Mei, and J. F. Klausner, Lattice Boltzmann models for the convection-diffusion equation: D2Q5 vs D2Q9, Int. J. Heat Mass Transfer **108**, 41 (2017).
[18] X. Shan and H. Chen, Lattice Boltzmann model for simulating flows with multiple phases and components, Phys. Rev. E **47**, 1815 (1993).
[19] Q. Li, K. H. Luo, Q. J. Kang, Y. L. He, Q. Chen, and Q. Liu, Lattice Boltzmann methods for multiphase flow and phase-change heat transfer, Prog. Energ. Combust. **52**, 62 (2016).
[20] T. Imamura, K. Suzuki, T. Nakamura, and M. Yoshida, Acceleration of steady-state lattice Boltzmann simulations on non-uniform mesh using local time step method, J. Comput. Phys. **202**, 645 (2005).
[21] H. Farhat and J. S. Lee, Fundamentals of migrating multi-block lattice Boltzmann model for immiscible mixtures in 2D geometries, Int. J. Multip. Flow **36**, 769 (2010).
[22] J. Huang, C. Yang, and X. Cai, A fully implicit method for lattice Boltzmann equations, SIAM J. Sci. Comput. **37**, S291 (2015).
[23] S. Osher and R. Sanders, Numerical approximations to nonlinear conservation laws with locally varying time and space grids, Math. Comp. **41**, 321 (1983).
[24] B. R. Hodges, A new approach to the local time stepping problem for scalar transport, Ocean Model. **77**, 1 (2014).
[25] L. Li, R. Mei, and J. F. Klausner, Boundary conditions for thermal lattice Boltzmann equation method, J. Comput. Phys. **237**, 366 (2013).
[26] L. Li, R. Mei, and J. F. Klausner, Heat transfer evaluation on curved boundaries in thermal lattice Boltzmann equation method, ASME J. Heat Transfer **136**, 012403 (2014).
[27] L. Li, N. AuYeung, R. Mei, and J. F. Klausner, Effects of tangential-type boundary condition discontinuities on the accuracy of lattice Boltzmann method for heat and mass transfer, Phys. Rev. E, **94**, 023307 (2016).
[28] J. D. Sterling and S. Chen, Stability analysis of lattice Boltzmann methods, J. Comput. Phys. **123**, 196 (1996).
[29] K. Guo, L. Li, G. Xiao, N. AuYeung, and R. Mei, Lattice Boltzmann method for conjugate heat and mass transfer with interfacial jump conditions, Int. J. Heat Mass Transfer **88**, 306 (2015).
[30] X. He and L.-S. Luo, Lattice Boltzmann model for the incompressible Navier-Stokes equation, J. Stat. Phys. **88**, 927 (1997).
[31] J. R. Womersley, Method for the calculation of velocity, rate of flow and viscous drag in arteries when the pressure gradient is known, J. Physiol. **127**, 553 (1955).